Model Development for Tube-in-Subfloor Radiant Floor Heating and Cooling

Sébastien Brideau, and Ian Beausoleil-Morrison
Carleton University, Ottawa, Ontario

Abstract

Radiant floor heating and cooling have the potential to decrease energy consumption in buildings. While some building energy simulation software include models for the thermally massive embedded tubes radiant floor systems, there are no models available for lightweight tube-in-subfloor systems. Tube-in-subfloor systems consist of a grooved wooden subfloor, and conductive fin. Tubes are laid in the grooves, and a floor cover is added on top.

This paper discusses the development of a transient tube-in-subfloor model and its implementation in ESP-r. This tube-in-subfloor radiant floor model uses the general approach of the existing embedded tube model in ESP-r and combines an analytical model of the tube with a two dimension finite difference model of the top layers of the floor construction. The calculated heat input to the floor construction is then used as an input to the ESP-r one dimension numerical model for heat conduction through building assemblies. The tube-in-subfloor model was compared with a transient two dimension finite element analysis model. A root mean square deviation of no more than 2.15 W/m^2 for the tested cases was found.

1 Introduction

Background information

Hydronic radiant floor heating and cooling have the advantage of using milder water temperatures than other types of heating or cooling systems. Energy savings can result from these milder water temperatures because the heating (or cooling) generation equipment can usually perform more efficiently and because low-temperature solar systems can be utilized. To be able to accurately predict the performance of hydronic radiant floor systems, accurate models are required. Models are readily available in various building simulation packages for embedded tube systems. Figure 1 shows a section of a typical embedded tube thin slab radiant floor. Hot water is pumped through the tubes during periods of heating demands and the heat diffuses through the gypsum up to the floor covering. The heat is then radiated and convected in the space. Similarly, during periods of cooling demand, cold water is pumped through the floor tubes. Embedded tube systems are heavier and may require a larger structure to support the extra weight. Additionally, because of the large thermal mass in typical embedded tubes radiant floors, controls can be problematic(A. K. Athienitis & Chen 2000). For example, during the heating season, a zone may be requiring heat at night. The floor will then be supplied with hot water all night and may be at relatively high temperatures come morning. If solar gains or other casual gains increase the space temperature in the morning, the supply of water will cease but the large amount of heat stored in

the floor will still be released in the space for potentially a few hours, resulting in overheating. These problems typically get exacerbated with large variations in casual gains and solar gains.

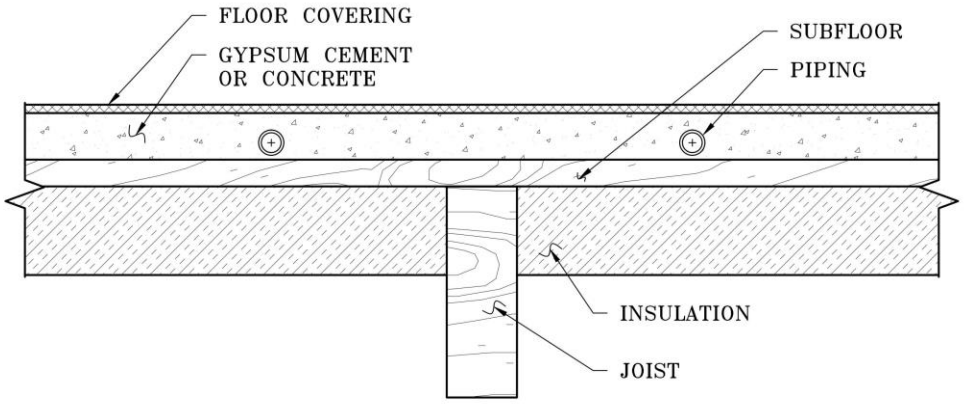

Figure 1: Section of an embedded tubes radiant floor

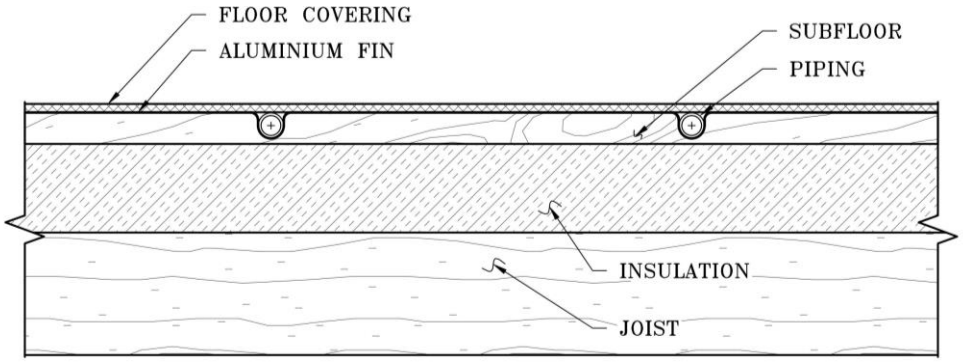

Figure 2: Section of a tube-in-subfloor radiant floor

Tube-in-subfloor systems can be used instead of embedded tube systems to reduce thermal mass. Figure 2 shows a section tube-in-subfloor radiant floor. Tube-in-subfloor systems consist of a grooved wooden subfloor, and conductive fins. Tubes are laid in the grooves, and a floor cover is added on top. Models for these types of radiant floors are however not currently available in building simulation software. This paper discusses the development and implementation of such a model for ESP-r.

Previous works

Historically, embedded tube systems were the most common type of radiant floor systems. Almost all of the models found in the literature were therefore initially developed for embedded tube systems.

To analyze radiant floors, one approach that has been used is to model the radiant floor as a fin (Kilkis et al. 1994; Ishino 1999). These steady state models are mostly used for sizing of systems. Recently, Carbonell et al. (2011) developed a model based on the work by Kilkis et al. (1994) coupled with a multilayer model to solve for the transient one-dimensional conduction of

the different layers. The fin equations used for this model were for steady-state conditions. The steady-state results were compared with experimental data, but there was no experimental data available to compare transient results.

Kattan et al. (2012) developed a radiant floor model that used finite difference in the water flow direction. This model used a fin thermal resistance to calculate the heat transferred to the room. The model was developed for an embedded tube system with a metallic sheet (or fin). The fin thermal resistance was based on steady-state fin equations. The results were compared with transient experimental results by Cho and Zaheer-uddin (1997). After review of the results provided in the paper, it is the opinion of the authors that the model does not agree with the experimental results.

Yeo & Kim (1997) developed a model for a fin radiant floor panel. The model consisted of two layers of insulation, underneath a fin. This arrangement is very similar to a tube-in-subfloor system, except that there was no floor cover. They modeled the floor using the finite difference method with an implicit scheme, but it is not clear how the tube was modeled and coupled to the finite difference model. Surface temperatures between the model and experimental results are reported to generally agree to within 0.5°C.

Laouadi (2004) developed a semi-analytical model for the ESP-r building simulation software. The model solved the conduction equation in two dimensions in the slab assuming a point source for heat flux and average slab properties. The calculated temperature of the point source was then used as the outside tube wall temperature to calculate the heat flux to the floor. This heat flux was communicated to the ESP-r building domain where it was injected as a heat source. The 1D transient conduction through the floor assembly was then calculated by using ESP-r's control-volume heat-balance method (refer to Clarke 2001 for details). This model was compared with results from a 2 dimension finite volume model with a fully implicit scheme. For a floor consisting of a floor cover, concrete slab, insulation, and gravel with a step input, the modelled average floor temperature was within 0.04°C of the numerical solution after 12 hours. The maximum floor surface temperature (directly above piping) was within 0.21°C of numerical solution while the minimum floor surface temperature (between tubes) was within 0.17°C. Most of this difference can be attributed to the use of an average thermal conductivity for the semi-analytical model calculations, the mesh size used in the numerical model, and the truncation error in the series solution to the semi-analytical model. The author also states that an excellent agreement is obtained when modelling a uniform slab (without covering and insulation), but does not state the magnitude of the difference between the two models.

Many other radiant floor models can be found in the literature (L. Hulbert et al. 1950; H. B. Nottage et al. 1953; Z. Zhang & Pate 1986; Z. Zhang & Pate 1987; A. Athienitis 1994; Jin et al. 2010; Strand et al. 2002; S.-Y. Ho 1992; S. Y. Ho et al. 1995). Because of a lack of experimental validation or cross model comparisons for many of the models, it is unclear which approaches produce the most accurate results.

There is a need for a model to accurately represent tube-in-subfloor systems in existing building simulation software. In addition to being accurate, this model should also require a minimal amount of computational effort in order to be adequate for use as part of full building simulation.

2 Model development

ESP-r building domain solution method

In order to solve for the transient heat transfer in a building's opaque fabric components, ESP-r uses a 1D finite difference approach (2D and 3D representations are possible, but rarely utilized). Each layer in a wall, floor, ceiling, or other opaque fabric component is represented by three nodes. Each layer is assumed to be homogenous. By default thermophysical properties are treated as constant, although thermal conductivity can be made to vary with temperature and moisture content.

ESP-r uses the Crank-Nicholson scheme to solve the 1D heat balance problem. The 1D heat conduction solution means that a single average temperature is calculated for every node and temperature gradients parallel to the surfaces are not considered. A similar approach is taken for surface nodes. For sake of brevity, details are omitted here and the interested reader is directed to work by Clarke (2001) for a detailed discussion.

Fin and cover finite difference conduction model

The approach taken for the new tube-in-subfloor model is similar to that of Laouadi (2004) discussed previously. The difference lies in the solution of the temperature field in the floor. Laouadi used average floor properties (conductivity, specific heat, density) and solved the two-dimensional conduction equation in the floor. This approach works well when all layers in the floor have similar thermal properties. When a fin with a much higher thermal conductivity is introduced, the results become inaccurate.

A finite difference model was developed to evaluate the temperature distribution in the fin and floor cover. Figure 3 shows the boundaries of the finite difference model. The finite difference model considers only the layers of floor cover and the fin. The subfloor and layers below it (e.g. insulation) are not considered in the model. The omission of those layers reduces the computational cost. This simplification also means that the thermal mass is underestimated in the finite difference model. A method to account for this simplification is discussed later in this section.

Only half of the distance between the tubes is modeled as it is assumed that the temperature distribution in the floor is symmetrical at a point halfway between two tubes, and at the center of each tube. An adiabatic boundary condition is used at those points.

Figure 4 shows a diagram of the finite difference model nodes and boundary conditions. The model is discretized in two layers of nodes, representing the fin, and the cover. The finite difference nodes representing the fin layer are located in the centre of the elements, while the nodes representing the floor cover layer are located at the boundary between the zone air and the floor. The tube is considered to be a heat source (or sink) (indicated by Q_c in the figure). The boundary conditions at the top surface are calculated based on the convective heat transfer coefficient calculated by the building domain. The radiant heat flux and solar heat flux are calculated by the ESP-r building domain and passed to the finite difference model.

To reduce the computational cost associated with the model, if there are multiple cover layers, they are represented as a single node in the finite difference model. An equivalent y-direction conductive heat transfer coefficient between fin nodes and cover nodes is calculated as one would a simple series thermal circuit, as seen in Equation (1). An equivalent x-direction conduction heat transfer coefficient between adjacent cover nodes is calculated using a thickness

weighted average conductivity in the same fashion as a parallel thermal circuit. This is seen in Equation (2). Equivalent density and specific heat of the cover elements are also calculated as thickness weighted averages shown in Equations (3) and (4).

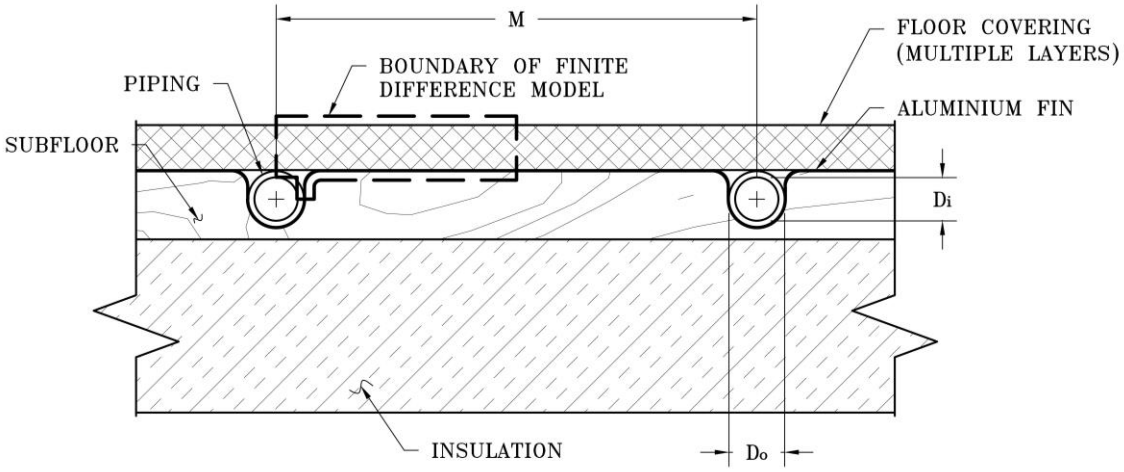

Figure 3: Section of a tube-in-subfloor radiant floor with boundaries of finite difference model

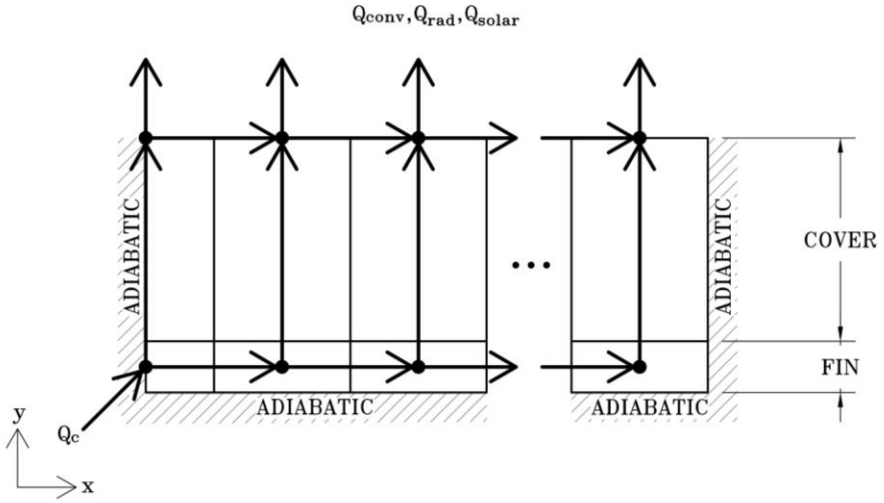

Figure 4: Finite difference model nodes and boundary conditions

$$h_{cond,y} = \left(\frac{\delta_{fin}}{2k_{fin}} + \sum_{i=1}^{N_{cover}} \frac{\delta_{i,cover}}{k_{i,cover}} \right)^{-1} \tag{1}$$

$$h_{cond,x,cover} = \frac{\sum_{i=1}^{N_{cover}} \delta_{i,cover} k_{i,cover}}{\Delta x \sum_{i=1}^{N_{cover}} \delta_{i,cover}} \tag{2}$$

$$\overline{\rho}_{cover} = \frac{\sum_{i=1}^{N_{cover}} \delta_{i,cover} \rho_{i,cover}}{\sum_{i=1}^{N_{cover}} \delta_{i,cover}} \quad (3)$$

$$\overline{C}_{cover} = \frac{\sum_{i=1}^{N_{cover}} \delta_{i,cover} C_{i,cover}}{\sum_{i=1}^{N_{cover}} \delta_{i,cover}} \quad (4)$$

The floor 2D finite difference model described so far is uncoupled from the building domain that solves the 1D conduction problem in building fabric. As mentioned above, the omission of the subfloor and insulation layers underestimates the thermal mass in the floor. Instead of using the 2D finite difference model temperature distribution as absolute values, the temperature distribution in the fin can be converted to deviation from the average layer temperature. As shown in Figure 5, the average fin temperature from the 2D model is calculated and the fin node temperatures are shifted so that the 2D average fin temperature matches the ESP-r building domain 1D conduction model fin node temperature. The floor cover surface node temperatures are similarly shifted to match the building domain 1D model surface temperature.

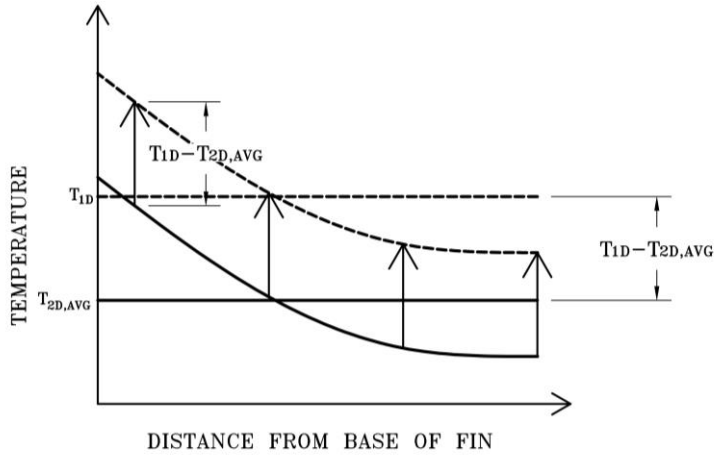

Figure 5: Shift of finite element temperature field to match average ESP-r temperature

Tube model

Laouadi (2004) described a detailed thermal model of a tube as part of a slab radiant floor model. For sake of brevity, only the resulting equations are included here and the interested reader is directed to the work by Laouadi (2004) for a detailed discussion of the pipe model.

Equation (5) shows the resulting discretized pipe conduction model for the fully implicit method.

$$(\alpha + \beta\Delta t)\overline{\Theta} - \alpha\overline{\Theta}^{old} - \Delta t\gamma = 0 \quad (5)$$

Where:

$$\overline{\Theta} = \frac{1}{L}\int_0^L \Theta dz \quad (6)$$

$$\Theta = T_f - T_{to} \tag{7}$$

$$\alpha = \frac{(\rho CA)_f}{UP} \tag{8}$$

$$\beta = \frac{\chi_1 L}{\chi_1 L - 1 + e^{-\chi_1 L}} \tag{9}$$

$$\gamma = \left(\frac{1 - e^{-\chi_1 L}}{\chi_1 L - 1 + e^{-\chi_1 L}} \right) \Theta_{in} - \frac{\chi_4}{UP} \frac{dT_{to}}{dt} \tag{10}$$

$$\Theta_{in} = T_{in} - T_{to} \tag{11}$$

$$\chi_1 = \frac{UP}{\dot{m} C_f} \tag{12}$$

$$\chi_4 = (\rho CA)_f + UPR_{cond,tube}(\rho CA)_{tube} \tag{13}$$

$$UP = \frac{1}{R_{conv,f} + R_{cond,tube}} \tag{14}$$

$$R_{conv,f} = \frac{1}{\pi D_{ti} h_f} \tag{15}$$

$$R_{cond,tube} = \frac{\ln(D_{to}/D_{ti})}{2\pi k_{tube}} \tag{16}$$

Equation (17) is then used to calculate the heat transferred to the floor.

$$Q_c = UPL\left\{ \overline{\Theta} - R_{conv,f} (\rho CA)_{tube} \frac{dT_{to}}{dt} \right\} \tag{17}$$

Implementation

Equation (5) requires knowledge of T_{to} which is not known. T_{to} can be approximated to be equal to the temperature of the fin node where the heat is injected in the finite difference model. Equations (5) and (17), and the finite difference model described in the previous section therefore require iteration to solve for the heat flux delivered to the floor at every time step.

Figure 7 shows a simplified flow chart of the model and it's interaction with the ESP-r building domain. At every time step, the ESP-r building domain calculates the 1D temperature distribution in the floor. The plant domain is then called, and Q_c is calculated based on previous time step or iteration values. The finite difference model is then solved using Q_c and boundary conditions at the floor surface (from the building domain). Then the temperature distribution is shifted up or down to match the 1D node temperatures from the ESP-r building domain and $\overline{\Theta}$ is calculated based on T_{to} being equal to the fin node where the heat is injected in the finite difference model. A convergence check is performed, and if the model has converged, it moves on to the next time step. If not, $\overline{\Theta}$ is used to recalculate Q_c.

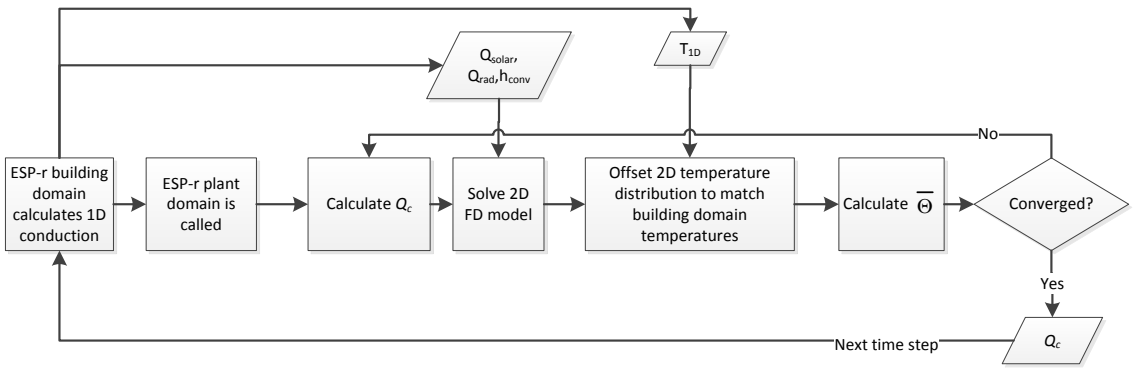

Figure 7: Flow chart of model

3 Results

The model described in this paper was compared with results predicted with a commercial 2D transient finite element package for two floor covering: hardwood, and tile. Figure 8 shows the finite element mesh and layers for the tile cover. Like the finite difference model, symmetry was used to reduce the required amount of nodes. Two different floor covers were modeled: hardwood and tile. The floor construction is shown in Table 1.

Table 1: Floor Construction

Layer	Specific heat (J/kg K)	Density (kg/m^3)	Conductivity (W/m K)	Thickness (m)
Insulation	960	100	0.036	0.076
Subfloor	1880	450	0.1	0.02794
Fin	900	2700	234	0.000635
Hardwood [a]	1210	600	0.14	0.01905
Thinset mortar [b]	780	1860	0.72	0.003175
Backer board [b]	840	1461	0.277	0.00635
Thinset mortar [b]	780	1860	0.72	0.003175
Tile [b]	837	2100	1.1	0.0127

a –Hardwood cover
b – Tile cover

Boundary conditions and time step

The boundary conditions were the same in the ESP-r simulation and in the finite element simulation. The floor surface was given a convective heat transfer coefficient of 5 W/m^{2}K with a constant zone air temperature at 15°C. The tube inner temperature was set to 45°C for the first 500 minutes, after which it is set to 30°C. In ESP-r, this was accomplished by providing an unrealistically high water flow rate at those temperatures such that the outlet temperature remained al-

most equal to the inlet temperature (within 0.01°C). The bottom boundary condition was adiabatic. The initial floor temperature was set to 15°C. No radiation heat transfer (long, or short wave) was considered. Time steps were 120 s for a total of 1280 minutes (21.33 hours).

Finite element mesh sensitivity

A mesh sensitivity analysis was performed with 120 s time steps. The total heat transfer from the floor to the surroundings was calculated for the first 78 minutes. The mesh refinement showed no significant changes in the results (<0.3%) after 3800 nodes for the tile floor cover. Similar results were found for the hardwood cover at 3706 nodes. Those meshes were therefore used for this study.

ESP-r finite difference mesh sensitivity

A mesh sensitivity was also performed in ESP-r with 120s time steps. The total heat transfer from the floor to the surroundings was calculated for the first 78 minutes. The mesh refinement showed no significant changes in the results (<0.3%) after 40 nodes.

Comparison

The heat flux from the floor surface to the surroundings as calculated by the FEA model and the ESP-r model are shown in Figure 9 for a tile floor cover. Forty data points were recorded with a root mean square deviation (RMSD) between the two models of 1.22 W/m^2. The heat flux for the first 39 time steps for tile cover are shown in Figure 10. For the first 39 time steps, the RMSD was 2.15 W/m^2.

Similarly, simulations with the hardwood cover were run. Results for the full length of the simulation (1280 minutes) and for the first 39 time steps are seen in Figures 11 and 12. The RMSD was 0.90 W/m^2 for the full length of the simulation and 1.83 W/m^2 for the first 39 time steps. These results imply that the ESP-r model does not agree as well with the FEA model in highly transient periods compared to steady state periods. Nonetheless, the ESP-r results in transient and steady state periods are quite close to the FEA results.

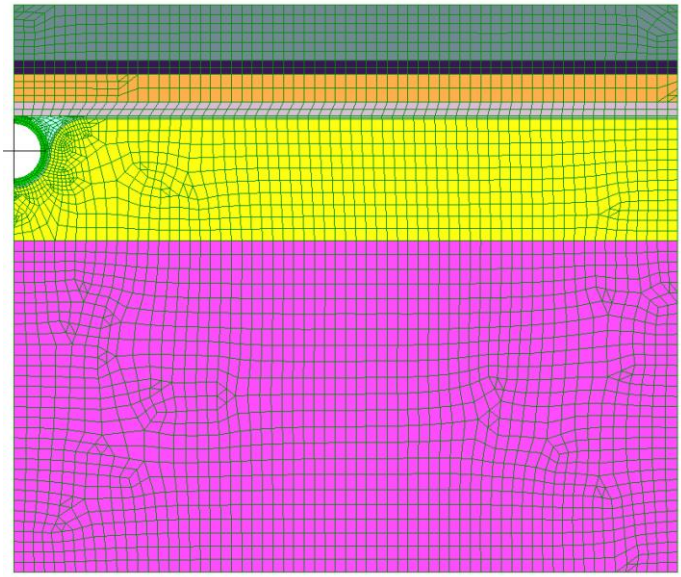

Figure 8: Finite element mesh for tile cover

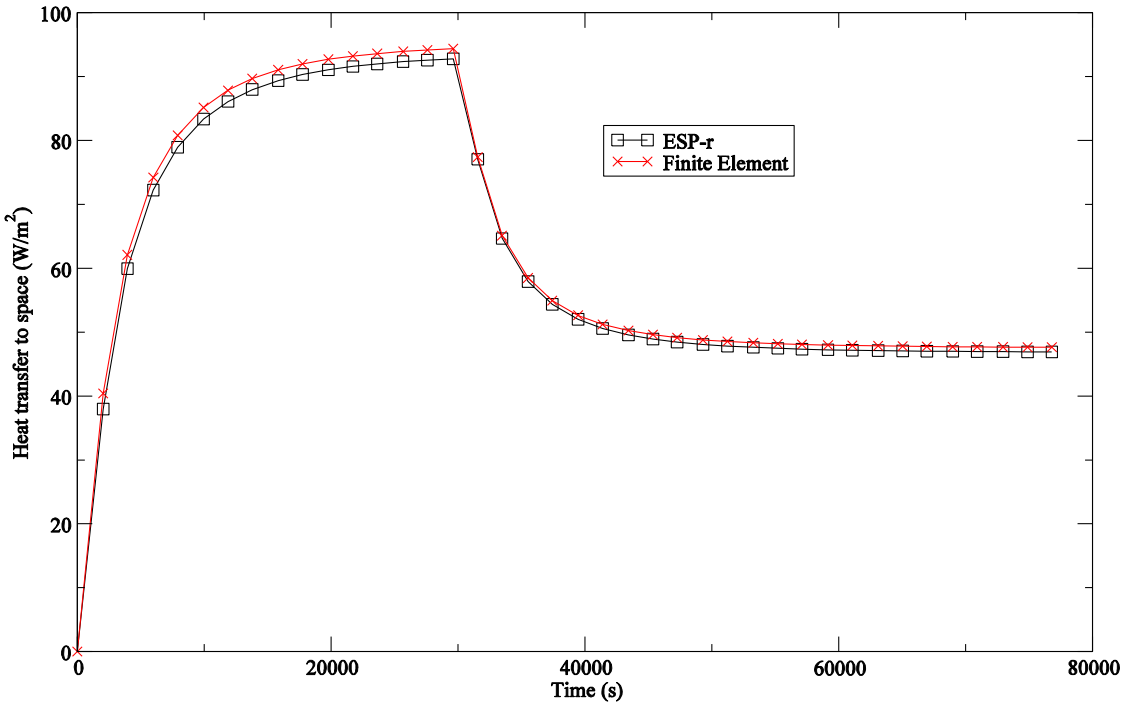

Figure 9: Comparison of ESP-r model with finite element model for tile cover and 1280 minutes

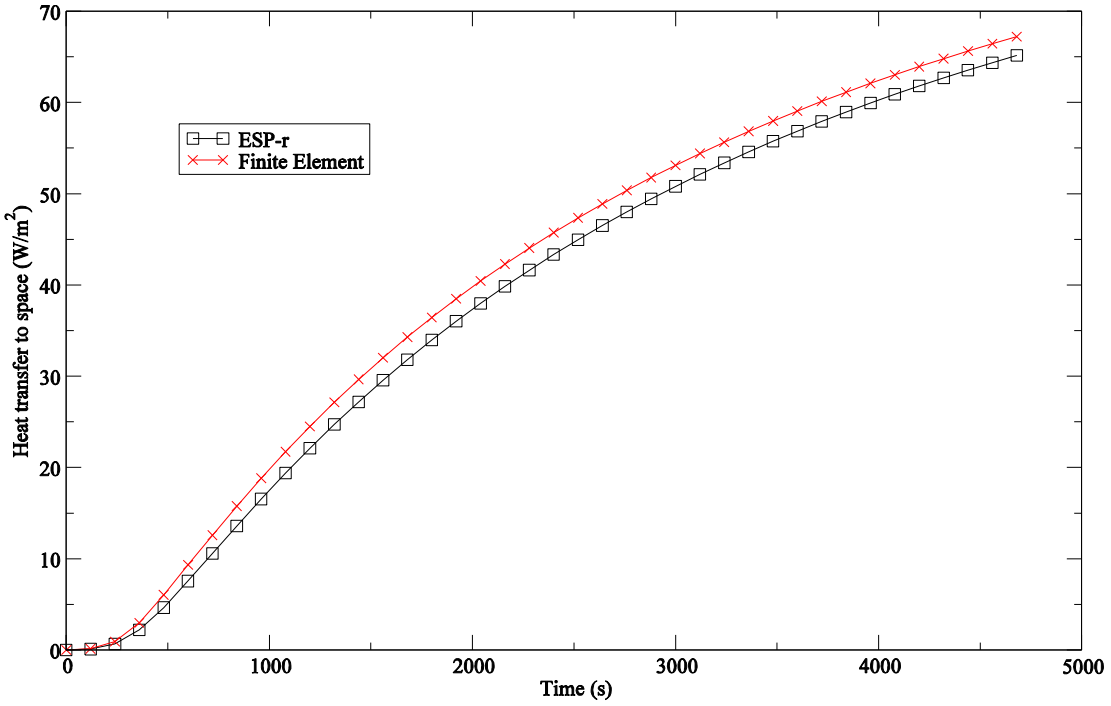

Figure 10: Comparison of ESP-r model with finite element model for tile cover and first 39 time steps (78 minutes)

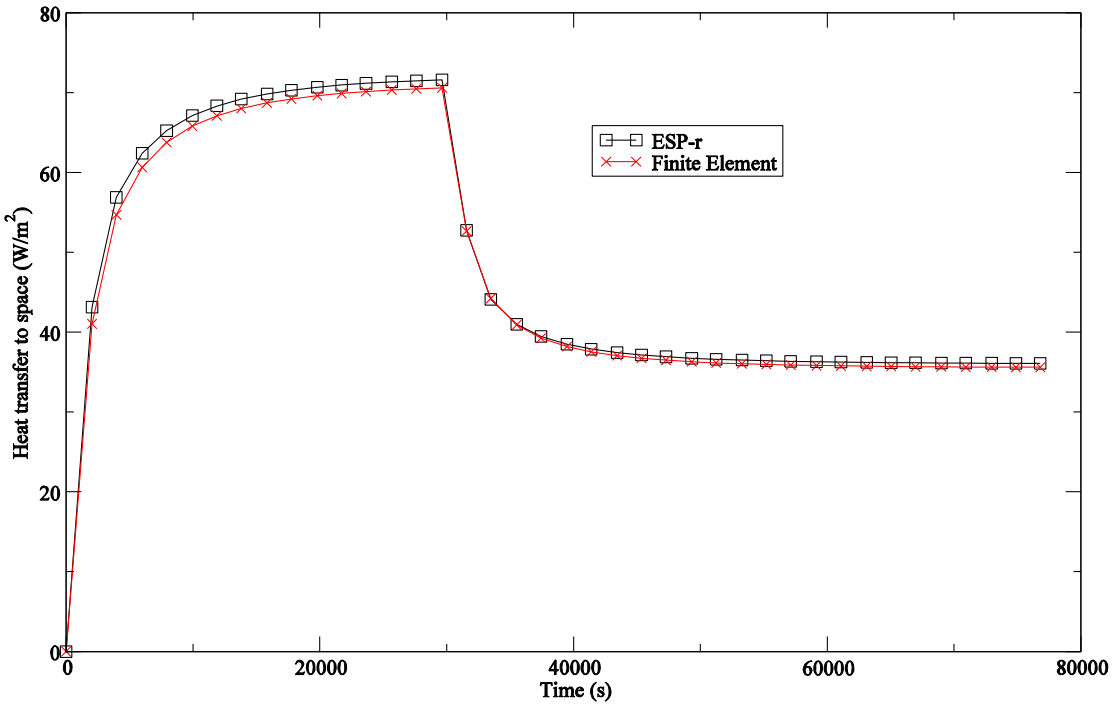

Figure 11: Comparison of ESP-r model with finite element model for hardwood cover and 1280 minutes

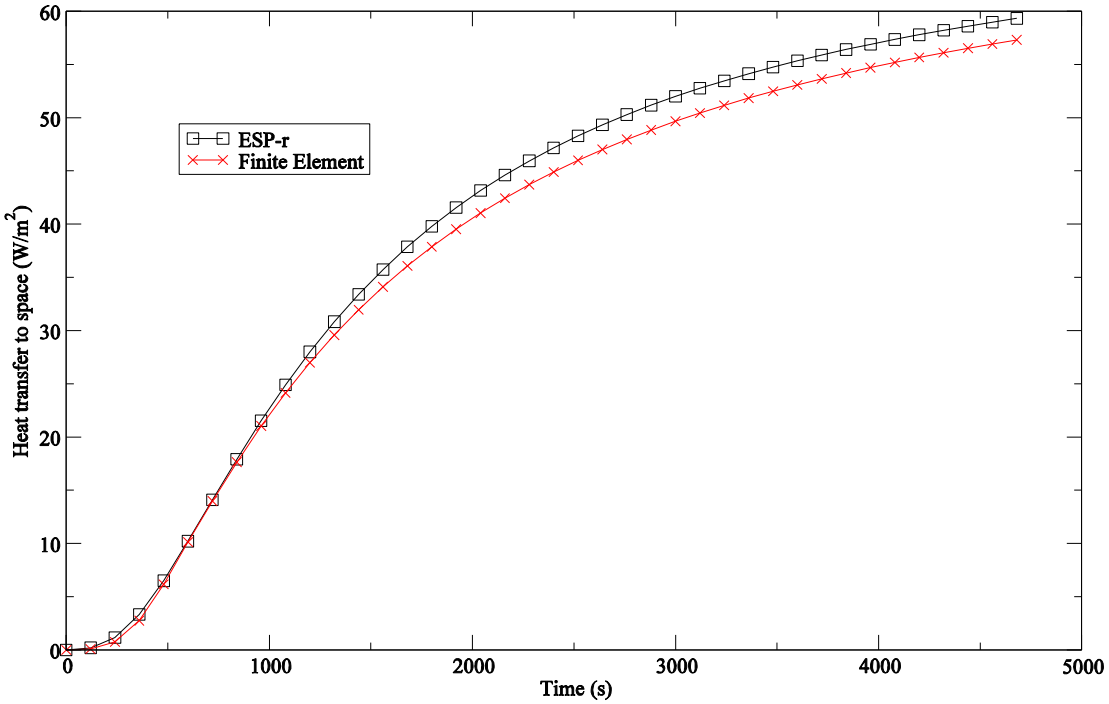

Figure 12: Comparison of ESP-r model with finite element model for hardwood cover and first 39 time steps (78 minutes)

Parametric Analysis

A parametric analysis was performed with the ESP-r model with a tile floor cover. The parameters investigated were: cover conductivity, cover thermal mass, tube conductivity, fin conductivity, fin thickness, subfloor conductivity and surface convective heat transfer coefficient. Each parameter was varied by +10% and -10% and a RMSD was calculated for all data points between the base case and the varied parameter case. Simulations were run in ESP-r with the same conditions as described previously. Table 2 shows the results.

Table 2: RMSD for various parameters perturbation

Parameter	RMSD for parameter +10% (W/m^2)	RMSD for parameter -10% (W/m^2)
k_{cover}	0.987	1.15
$(\rho C)_{cover}$	0.815	0.857
k_{tube}	0.684	0.812
k_{fin}	1.017	1.024
t_{fin}	0.969	1.16
$k_{subfloor}$	0.277	0.299
h_{cover}	4.06	4.36

Considering that the RMSD between the FEA model and the ESP-r model for the tile cover was 1.22 W/m^2 for the full simulation (1280 minutes), it can be seen that varying some of the parameters by 10% would result in similar results. The fin thickness and conductivity, and the cover conductivity all have RMSD around $1W/m^2$ for a 10% change. The heat transfer coefficient is much higher at around 4 W/m^2. This is of interest because in a situation where one wants to model a building with a radiant floor, the various parameters related to floor are usually not known to a great level of certainty. This analysis shows that the difference between the FEA results and the ESP-r results is similar or smaller to the uncertainty one would get from the input parameters or heat transfer coefficient.

4 Conclusions

The development of a tube-in-subfloor radiant floor heating and cooling model in ESP-r was discussed. The model consists of an analytical solution to the tube heat transfer coupled with a 2D finite difference conduction model. A RMSD of no more than 2.15 W/m^2 was found between this new model and a 2D transient finite difference analysis for the tested cases.

It was found that the new model deviated slightly from the FEA solution during highly transient periods but the results were still deemed reasonable. Furthermore, a parametric analysis performed in ESP-r showed that changing model parameters by 10% can change the results by a larger amount than the difference between the FEA and ESP-r results.

5 Future work

Future work involves comparing modeled results with experimental data. An experimental house will be used to run a set of experiments, and this new model will be compared with those results.

6 Acknowledgements

The authors would like to thank the NSERC Smart Net-Zero Energy Buildings Research Network for funding of this work.

7 Nomenclature

A	Cross sectional area [m^2]
C	Specific heat [J/kg·K]
D	Diameter [m]
h	Heat transfer coefficient [$W/m^2 \cdot K$]
k	Thermal conductivity [W/m·K]
L	Length of circuit [m]
$\dot{m}$	Mass flow rate [kg/s]
N_{cover}	Amount of cover layers [-]
Q	Heat transfer rate [W]
R	Thermal resistance per unit tubing circuit length [m·K/W]
T	Temperature [K]
t	Time [s]
UP	Product of tubing overall heat conductance and perimeter [W/m·K]
z	Distance in direction of fluid flow [m]

Greek letters

Δx	Width of finite difference element [m]
Δt	Time step size [s]
δ	Floor layer thickness [m]
Θ	Temperature gradient between fluid and outer tube [K]
ρ	Density [kg/m^3]

Subscripts and superscripts

b	From boiler to circuit fluid
c	From tubing to floor
cond	Conduction
conv	Convection
cover	Floor cover
f	Fluid
f-tube	From fluid to tubing
in	Inlet
old	Previous time step
ti	Inner tubing
to	Outer tubing
x	X-axis, parallel to floor
y	Y-axis, perpendicular to floor

8 References

Athienitis, A., 1994. Numerical model of floor heating system. *ASHRAE Transactions*, 100(1), pp.1024–1030.

Athienitis, A.K. & Chen, Y., 2000. The effect of solar radiation on dynamic thermal performance of floor heating systems. *Solar Energy*, 69(3), pp.229–237.

Carbonell, D., Cadafalch, J. & Consul, R., 2011. A transient model for radiant heating and cooling terminal heat exchangers applied to radiant floors and ceiling panels. *ISES Solar World Congress 2011 Proceedings*.

Cho, S.-H. & Zaheer-uddin, M., 1997. Temperature regulation of radiant floor heating systems using two-parameter on-off control: An experimental study. *ASHRAE Transactions*, 103(1), pp.966–982.

Clarke, J.A., 2001. *Energy Simulation in Building Design* 2nd ed., Oxford: Butterworth-Heinemann.

Ho, S.-Y., 1992. *Simulation of the dynamic behaviour of a hydronic floor heating system*. University of Alberta.

Ho, S.Y., Hayes, R.E. & Wood, R.K., 1995. Simulation of the Dynamic Behaviour of a Hydronic Floor Heating System. *Heat Recovery Systems and CHP*, 15(6), pp.505–519.

Hulbert, L., Nottage, H. & Franks, C., 1950. Heat flow analysis in panel heating or cooling sections. *Heating, Piping and Air Conditioning*.

Ishino, H., 1999. Research on calculation method of thermal design load in radiant heating and cooling systems. *International Building Performance Simulation Association Conference Proceedings*.

Jin, X., Zhang, X. & Luo, Y., 2010. A calculation method for the floor surface temperature in radiant floor system. *Energy and Buildings*, 42(10), pp.1753–1758.

Kattan, P., Ghali, K. & Al-Hindi, M., 2012. Modeling of under-floor heating systems: A compromise between accuracy and complexity. *HVAC & R Research*, (July), pp.37–41.

Kilkis, Í., Sager, S. & Uludag, M., 1994. A simplified model for radiant heating and cooling panels. *Simulation Practice and Theory*, 2(2).

Laouadi, A., 2004. Development of a radiant heating and cooling model. *Building and Environment*, 39(4), pp.421–431.

Nottage, H.B. et al., 1953. Heat Flow Analysis in Panel Heating or Cooling sections. Case II–Floor Slab on Earth with Uniformly Spaced Pipes or Tubes at the Slab-Earth Interface. *ASHVE Heating, Piping and Air Conditioning*.

Strand, R.K., Ph, D. & Pedersen, C.O., 2002. Modeling Radiant Systems in an Integrated Heat Balance Based Energy Simulation Program. *ASHRAE Transactions*, 108(2).

Yeo, M. & Kim, K., 1997. A Study on the Thermal Performance Simulation to Evaluate the Prefabricated Radiant Floor Heating Panels. In *Proceedings of the 5th International IBPSA Conference*. Prague.

Zhang, Z. & Pate, M.B., 1986. A numerical study of heat transfer in a hydronic radiant ceiling panel. *ASME Proceedings - Heat Transfer Division*, 62.

Zhang, Z. & Pate, M.B., 1987. A semi-analytical formulation of heat transfer from structures with embedded tubes. *ASME Proceedings - Heat Transfer Division*, 78, pp.17–25.